Out-of-Focus Spatial Map Imaging of Magnetically Deflected Sodium-Doped Ammonia Clusters

D. P. Borgeaud dit Avocat, H. Yang, A. Nitsche, J. Wenger, B. L. Yoder and R. Signorell*

Experimental Calibration and Validation

Cluster generation

For the generation of toluene, methanol, and water clusters, a bubbler preceding the nozzle was utilized. The bubbler was filled with the respective liquid and heated to temperatures of $25°C$, $95°C$, and $115°C$, respectively. Correspondingly, the nozzle was heated to $45°C$ for toluene, $100°C$ for methanol, and $140°C$ for water, to ensure optimal vaporization and subsequently cluster formation. After passing the first skimmer (S1) (1.5 mm diameter), the resulting cluster beam of methanol and water was doped with a single sodium atom as it traversed an oven with sodium that was heated to $230°C$.

Experimental Calibration

To calibrate the magnification factor of the position, we performed measurements to determine the width of the molecular beam along the deflection/laser axis (z), where the velocities of our clusters are negligibly small (Fig. S1). The spatial magnification of positions can be expressed by $M_r = w_d/w_i$, where w_d and w_i are the widths, approximated as 3σ, of the spatial distributions at detection and ionization, respectively.
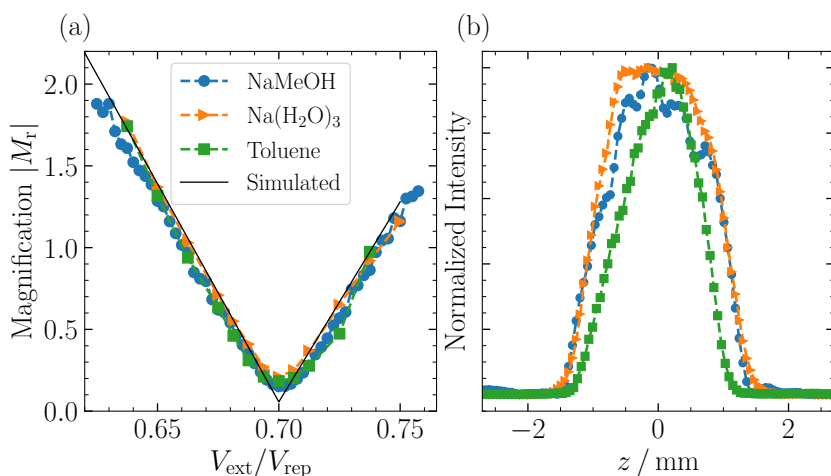

Fig. S1 Spatial Map Imaging calibration results. (a) Measured magnifications for Na(MeOH), Na(H$_2$O)$_3$, and toluene, along with the simulated magnification for Na(MeOH), are plotted as a function of the extractor repeller voltage ratio. (b) The measured distributions at detection for Na(MeOH), Na(H$_2$O)$_3$, and toluene at a magnification of $M_r = 1$ are shown. It is noteworthy that due to the rearrangement of trajectories in the sodium oven, the width at ionization is larger for sodium-doped than for the undoped species.

The width of the distribution at ionization was calculated by taking the diameter of S3 and adding the divergence of the molecular beam. For measurements conducted using undoped toluene, the divergence angle was determined by considering the nozzle to be a point source and the radius of S3 to be the limiting aperture, resulting in an acceptance angle of $\alpha_{Tol} = 0.075°$ and a corresponding width at ionization (3σ) of $w_{i,Tol} = 2.48\,mm$. However, when sodium-doped clusters were used, the size at ionization was larger due to trajectory rearrangement resulting from collisions between the solvent clusters and sodium atoms in the oven. In this case, the divergence angle was determined by S2 and S3, resulting in $\alpha_{NaX} = 0.164°$ and a cluster beam width of $w_{i,NaX} = 3.05\,mm$ at ionization. The disparity in beam divergence between toluene and NaX clusters can be observed in Fig. S1, which was obtained at a voltage ratio of $V_{ext}/V_{rep} = 0.66$. This ratio corresponds to the point where the width of

Department of Chemistry and Applied Biosciences, ETH Zurich, CH-8093 Zurich, Switzerland. E-mail: ruth.signorell@phys.chem.ethz.ch

the distribution at the detector matches that at the ionization point ($M_r = 1$).

Fig. S1 illustrates the different magnifications obtained for toluene, sodium-doped clusters, and SIMION simulations for point particles with the mass of Na(MeOH) clusters. The various measurements exhibit good agreement, highlighting that M_r is mass independent.

Laser size determination

In this section, we retrieve the laser size in the propagation (x)-direction, which is perpendicular to the deflection (z)-direction. The spatial distribution in the x-direction is determined by the intensity profile of the laser, under the conditions of a continuous supersonic expansion. However, it is important to note that in the x-direction, the velocity distribution is much broader ($\Delta v_x \approx 500\,\mathrm{m\,s^{-1}}$) than in the z-direction ($\Delta v_z \approx 2\,\mathrm{m\,s^{-1}}$). Consequently, to accurately retrieve the spatial distribution at ionization, it becomes necessary to deconvolve the velocity distribution from the distribution measured at the detector, as described in Eq. 3.

This deconvolution is accomplished by assuming Gaussian distributions for both the spatial distribution, corresponding to the laser's intensity profile, and the velocity distribution, as shown in Fig. 5. The convolution of these two Gaussian distributions results in another Gaussian function. This relationship enables us to formulate Eq. 3 for the variance (σ^2) at the detector as follows:

$$\sigma_{r_d}^2 = M_r^2\,\sigma_{r_i}^2 + M_v^2\,\sigma_{v_i}^2. \tag{S1}$$

Using the Na(MeOH) data presented in Fig S1, we can use the SMI measurements to calculate the size of the laser beam using equation S1 as follows: At VMI conditions, where $M_r = 0$, we can directly extract the velocity distribution $M_{v,\mathrm{VMI}}^2\,\sigma_{v_i}^2$ from the measurements (Fig. 5). For other extractor/repeller ratios, we made the approximation that the magnification of velocities remains constant ($M_v \approx M_{v,\mathrm{VMI}}$). With this approximation, we were able to rewrite equation S1 as:

$$\sigma_{r_i} \approx \sqrt{\frac{\sigma_{r_d}^2 - M_{v,\mathrm{VMI}}\sigma_{v_i}^2}{M_r^2}},. \tag{S2}$$

Using M_r given in Fig. S1 and excluding measurements obtained close to VMI within a range of $V_{\mathrm{ext}}/V_{\mathrm{rep}} = 0.70 \pm 0.03$, we determined a mean standard deviation of $\sigma_{r_i} = 0.75(6)\,\mathrm{mm}$ or $\mathrm{FWHM}_{r_i} = 1.77(14)\,\mathrm{mm}$. The exclusion of values close to VMI is justified as M_r in that region is extremely small, rendering it difficult to extract meaningful information on the spatial distribution.

This measurement is to be compared with independent measurements of the size of our collimated laser beam at both the entrance and exit windows of our vacuum chamber. The laser size was determined using the razor blade method, yielding a full width at half maximum of $\mathrm{FWHM}_{\mathrm{en}} = 1.62(7)\,\mathrm{mm}$ and $\mathrm{FWHM}_{\mathrm{ex}} = 1.63(5)\,\mathrm{mm}$ at the entrance and exit, respectively.

The values obtained with the razor blade method and those derived from our SMI measurements are in good agreement and confirm the validity of the SMI approach.

Error calculation of chi-square fit

The standard deviation of the relaxation time in this work τ_{SMI} is calculated using the principles of Gaussian error propagation and the minimisation of the chi-square function. The formula takes into account the distribution of the data points. The formula is given by:

$$\sigma(\tau_{\mathrm{SMI}}) = \sqrt{\left(\frac{d^2\chi^2(\tau)}{d\tau^2}\right)^{-1}}\sqrt{\frac{\chi^2(\tau_{\mathrm{SMI}})}{(N-1)}}. \tag{S3}$$

In this equation, $\sigma(\tau_{\mathrm{SMI}})$ represents the standard deviation of the optimal relaxation time parameter. The term $\frac{d^2\chi^2(\tau)}{d\tau^2}$ is the second derivative of the function $\chi^2(\tau)$ evaluated at τ_{SMI}, which reflects the curvature of $\chi^2(\tau)$ at the minimum. The chi-square value at the minimum, $\chi^2(\tau_{\mathrm{SMI}})$, is divided by $N-1$, where N is the number of data points. This scaling adjusts the variance derived from the error propagation to reflect the observed variance in the data. For a sufficiently large number of data

points N, the ratio $\frac{\chi^2(\tau_{\mathrm{SMI}})}{(N-1)}$ converges towards one.

Quantum Chemical Calculations

In a first step, the dispersion corrected ωB97XD density functional with a 6-31+G* basis set was used to optimize cluster geometries and find potential isomers. In the second step, the converged minimal energy structures are reoptimized with MP2 calculations with an aug-cc-PVDZ basis set and additional harmonic frequency calculations are carried out. The results for $Na_2(NH_3)_1$, $Na_3(NH_3)_1$, $Na_3(NH_3)_2$ are presented in this section

$Na_2(NH_3)_1$

For $Na_2(NH_3)_1$ only a singlet structure converged with C_{3v} symmetry. The Na-Na bond length is 3.24 Å, whereas the Na-N bond length is 2.52 Å. The Na-Na-N angle is 180° leading to the c3v symmetry.

Table S1 $Na_2(NH_3)_1$: Rotational constants of MP2-optimized singlet cluster structures (aug-cc-pVDZ) alongside their point groups (PG). The energy differences between structural isomers, denoted as ΔE, are also provided.

$Na_2(NH_3)_1$	ΔE/meV	PG	A/cm^{-1}	B/cm^{-1}	C/cm^{-1}
(a)	0	C_{3v}	6.29	0.05	0.05

(a)

Fig. S2 MP2/aug-cc-pVDZ optimized geometry for the $Na_2(NH_3)_1$ singlet structure.

Na$_3$(NH$_3$)$_1$

For Na$_3$(NH$_3$)$_1$ multiple isomers converged. All structures we converged for the Na$_3$(NH$_3$)$_1$ cluster are asymmetric rotors with the highest point groups being C$_s$, and in each isomer, the N atom of the NH$_3$ lies in the plane defined by the 3 Na atoms, with the nitrogen assuming various positions around the Na$_3$ manifold. For the various isomers the Na-N bond is similar (≈ 2.5 Å). The bond lengths and angles of the scalene triangle spanned by the three Na atoms change slightly for the different isomers, where the largest angle of the triangle (closest to the ammonia) is $\approx 72 \pm 0.5°$

Table S2 Na$_3$(NH$_3$)$_1$: Rotational constants of MP2-optimized singlet cluster structures (aug-cc-pVDZ) alongside their point groups (PG). The energy differences between structural isomers, denoted as ΔE, are also provided.

Na$_3$(NH$_3$)$_1$	ΔE/meV	PG	A/cm^{-1}	B/cm^{-1}	C/cm^{-1}
(a)	0	C$_s$	0.09	0.04	0.03
(b)	10	C$_s$	0.09	0.05	0.03

(a)   (b)

Fig. S3 MP2/aug-cc-pVDZ optimized geometries for selected Na$_3$(NH$_3$)$_1$ isomers.

Na$_3$(NH$_3$)$_2$

For Na$_3$(NH$_3$)$_2$, four isomers converged, with two isomers being isoenergetic. The angles and bond lengths for the different triangles spanned by the three Na atoms vary significantly. For structures (a) and (b), the three sodium atoms form an isosceles triangle, whereas the triangle in structure (c) is scalene

Table S3 Na$_3$(NH$_3$)$_1$: Rotational constants of MP2-optimized cluster structures (aug-cc-pVDZ) alongside their point groups (PG). The energy differences between structural isomers, denoted as ΔE, are also provided.

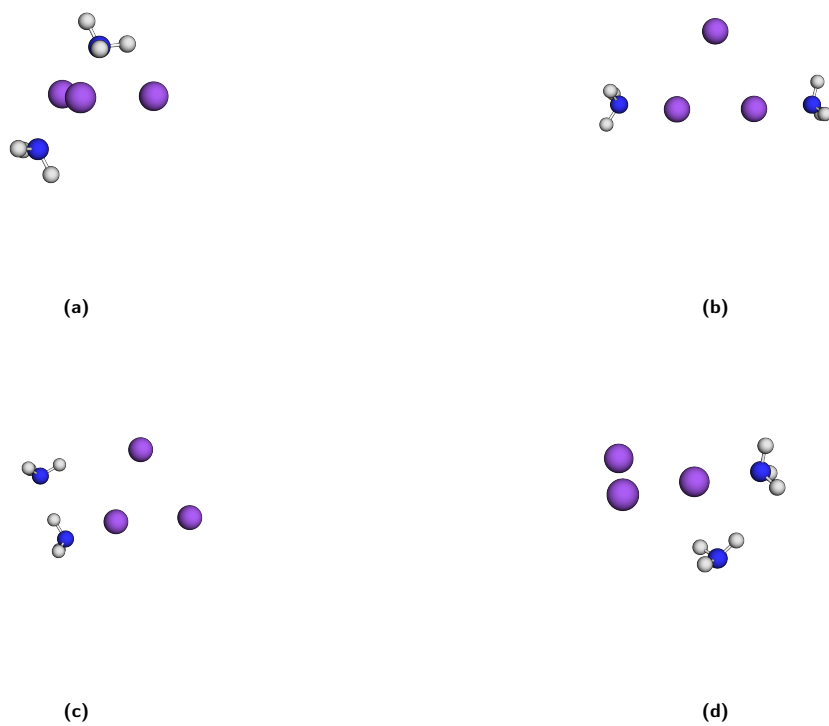| Na$_3$(NH$_3$)$_2$	ΔE/meV	PG	A/cm^{-1}	B/cm^{-1}	C/cm^{-1}
(a)	0	C$_2$	0.05	0.04	0.03
(b)	2	C$_{2v}$	0.08	0.022	0.018
(c)	186	C$_s$	0.08	0.03	0.020
(d)	424	C$_s$	0.05	0.03	0.025

(a)

(b)

(c)

(d)

Fig. S4 MP2/aug-cc-pVDZ optimized geometries for selected $Na_3(NH_3)_2$ isomers.